



Article

Biopolymeric Ni₃S₄/Ag₂S/TiO₂/Calcium Alginate Aerogel for the Decontamination of Pharmaceutical Drug and Microbial Pollutants from Wastewater

Rajeev Kumar ^{1,*} , Mohammad Oves ², Mohammad Omaish Ansari ³ , Md. Abu Taleb ¹ ,
Mohamed A. Barakat ^{1,*} , Mansour A. Alghamdi ¹ and Naief Hamoud Al Makishah ¹

- ¹ Department of Environmental Sciences, Faculty of Meteorology, Environment and Arid Land Agriculture, King Abdulaziz University, Jeddah 21589, Saudi Arabia
² Central of Excellence in Environmental Studies, King Abdulaziz University, Jeddah 21589, Saudi Arabia
³ Central of Nanotechnology, King Abdulaziz University, Jeddah 21589, Saudi Arabia
* Correspondence: rsingh@kau.edu.sa (R.K.); mabarakat@gmail.com (M.A.B.)

Abstract: The ubiquitous presence of pharmaceutical drugs and microbes in the water is leading to the development of drug resistant microbes. Therefore, efficient materials that can remove or inactivate the drug and microbe contaminants are required. In this work, nickel sulfide/calcium alginate (Ni₃S₄/CA), silver sulfide/calcium alginate (Ag₂S/CA), modified titanium dioxide/calcium alginate (TiO₂/CA), and Ni₃S₄/Ag₂S/TiO₂/calcium alginate (Ni₃S₄/Ag₂S/TiO₂/CA) aerogels have been synthesized for the removal of the oxytetracycline (OTC) drug and microbial contaminants from real beverage industry wastewater. The results revealed that Ni₃S₄/Ag₂S/TiO₂/CA aerogel is highly efficient for OTC adsorption and inactivation of microbes compared to Ni₃S₄/CA, Ag₂S/CA and TiO₂/CA aerogels. The OTC adsorption depends greatly on the solution pH, and optimum OTC removal was observed at pH 6 in its zwitterionic (OTC[±]) form. The formation of H-bonding and n-π electron donor-acceptors is possible to a considerable extent due to the presence of the double bond benzene ring, oxygen and nitrogen, sulfur-containing functional groups on the OTC molecules, and the Ni₃S₄/Ag₂S/TiO₂/CA aerogel. Based on the statistical analysis, root-mean-square deviation (RMSD), chi square (χ²) values, and higher correlation coefficient (R²) values, the Redlich–Peterson isotherm model and Elovich kinetic model are most suited to modelling the OTC adsorption onto Ni₃S₄/Ag₂S/TiO₂/CA. The prepared aerogels' excellent antimicrobial activity is observed in the dark and with solar light irradiation. The zone of inhibition analysis revealed that the antimicrobial activity of the aerogels is in the following order: Ni₃S₄/Ag₂S/TiO₂/CA > TiO₂/CA > Ag₂S/CA > Ni₃S₄/CA, respectively. Moreover, the antimicrobial results demonstrated that reactive oxygen species, electrons, and active radical species are responsible for growth inhibition and killing of the microbes. These results indicated that Ni₃S₄/Ag₂S/TiO₂/CA aerogel is highly efficient in decontaminating pollutants from wastewater.

Keywords: Ni₃S₄/Ag₂S/TiO₂/CA aerogel; drug adsorption; microbial decontamination; photocatalysis; mechanism



Citation: Kumar, R.; Oves, M.; Ansari, M.O.; Taleb, M.A.; Baraka, M.A.; Alghamdi, M.A.; Makishah, N.H.A. Biopolymeric Ni₃S₄/Ag₂S/TiO₂/Calcium Alginate Aerogel for the Decontamination of Pharmaceutical Drug and Microbial Pollutants from Wastewater. *Nanomaterials* **2022**, *12*, 3642. <https://doi.org/10.3390/nano12203642>

Academic Editor: Marco Stoller

Received: 13 September 2022

Accepted: 13 October 2022

Published: 17 October 2022

Publisher's Note: MDPI stays neutral with regard to jurisdictional claims in published maps and institutional affiliations.



Copyright: © 2022 by the authors. Licensee MDPI, Basel, Switzerland. This article is an open access article distributed under the terms and conditions of the Creative Commons Attribution (CC BY) license (<https://creativecommons.org/licenses/by/4.0/>).

1. Introduction

The complex nature of the wastewater released from industries and domestic activity is challenging traditional wastewater treatment methods. Municipal wastewater is now more complex and contains organic, inorganic, and microbial pollutants. In fact, the presence of pharmaceuticals and microbes is very common in municipal wastewater. The presence of pharmaceutical drugs and bacteria is not safe for human health because bacteria may develop resistance to the drugs [1]. The problem of pharmaceuticals and microbial pollution is growing as the consumption and release of these pollutants surges. In this context, nanomaterials derived from metal oxides, carbon, polymers, biopolymers, solid

waste, etc. are being investigated for the decontamination of pharmaceuticals and microbial pollutants [2]. The removal of these pollutants using nanomaterials is mainly controlled by surface interaction or decomposition. However, synthesizing nanomaterials with high decontamination and reusable properties is still challenging.

Metal sulfides and their composite materials are widely investigated in energy, catalysis, and environmental remediation applications [3,4]. Previous studies reported that sulfides of copper, silver, molybdenum, zinc, nickel, selenium, etc., had been used to remove heavy metals and organics, and for disinfection [5]. The high efficacy of the metal sulfides for removal of contaminants is due to their structure, with many active sites and defects, S and metal edge sites, and basal plane sites [6]. In metal sulfides, metals and sulfur atoms are bonded chemically to make a stable structure. Therefore, the properties and structure of the metal sulfide can be tuned to develop an efficient material for water purification. Silver and nickel sulfides are well-known materials for environmental remediation applications. Kumar et al. [7] synthesized polyacrylamide grafted gum karaya/NiS/Ni₃S₄ bio-nanocomposite to remove rhodamine 6G, showing a very high adsorption capacity (1244.71 mg/g). Alongside the adsorption properties, the antimicrobial properties of pure or Ni_xS_y-based composites have been reported in the literature. Hosseini et al. [8] fabricated a NiS-SiO₂ nanocatalyst and investigated its efficacy as a photocatalyst and antimicrobial agent. The synthesized material was highly stable in UV light and performed better than the parent materials. Highly stable hollow/solid Ag₂S/Ag heterodimers were synthesized by ion exchange and photo-assisted reduction. Ag₂S/Ag heterodimers showed excellent deactivation properties of *Escherichia coli* K-12 [9]. Besides the antimicrobial application, Ag₂S@Ag nanoparticles have been investigated for superior dye adsorption performance by Zhang et al. (2016) [10]. Gupta et al. [11] used the Ag₂S-chitosan nanohybrid for Clindamycin antibiotic sorption. The electrostatic interaction between the drug and nanohybrid was a major driving force in the sorption process. The adsorption of the organic pollutants onto metal sulfide is controlled by ionic bond formation, hydrogen bonding, and electron donor-acceptor mechanisms. At the same time, the microbes' deactivation occurs by cell destruction caused by eluted metal ions' cytotoxicity and active radicals produced by the material. Although the leaching of the metal ions from the materials showed excellent microbial deactivation, the nanocatalyst's stability is compromised and reusability of the material is limited [9]. Therefore, the development of sustainable and economical metal sulfide-based materials with high stability, easy separation from the aqueous solution, and excellent adsorption and microbial properties for wastewater purification is needed.

Developing new mixed metal sulfides or combinations with metal oxides or polymers having good adsorption and antibacterial effects could have advantages over the single component materials. Therefore, synthesizing the mixed silver and nickel sulfide (Ni₃S₄/Ag₂S) on a TiO₂ surface could be a new approach for the fabrication of a new material (Ni₃S₄/Ag₂S/TiO₂) for the pharmaceutical drug and microbial decontamination for wastewater. However, separating the powdered Ni₃S₄/Ag₂S/TiO₂ nanocomposite might be challenging. In this context, synthesizing an aerogel could be a better approach to develop porous materials that can easily be separated from the aqueous solution and enhance the water purification capacity of the immobilized material. Polysaccharides like alginate have special advantages because of their structural and physicochemical properties, biocompatibility, environmentally friendliness, good adsorptive and antimicrobial capacity [12]. The immobilization of Ni₃S₄/Ag₂S/TiO₂ nanocomposite within the alginate matrix could show higher adsorption and microbial decontamination properties, and its aerogel can be easily isolated from the wastewater after use. Herein, Ni₃S₄/Ag₂S/TiO₂/calcium alginate (Ni₃S₄/Ag₂S/TiO₂/CA) aerogel has been synthesized to remove the oxytetracycline (OTC) drug and promote microbial decontamination of waste water from the beverage industry. A detailed mechanism has been proposed to understand the adsorption and microbial decontamination behaviour of the Ni₃S₄/Ag₂S/TiO₂/CA.

2. Materials and Method

2.1. Materials

Sodium alginate was received from Techno Pharma (Delhi, India). TiCl_4 , Na_2S , NiCl_2 , silver acetate, and CaCl_2 were obtained from Sigma-Aldrich (Saint-Louis, MO, USA), and BDH Chemicals Ltd. (Mumbai, India). TiO_2 (P25) was obtained from Alfa Aesar (Haverhill, MA, USA).

2.2. Synthesis

2.2.1. Modification of TiO_2

Initially, 5 g TiO_2 (P25) was mixed with 70 mL 10 M NaOH and heated at 120 °C in a hydrothermal reactor for 24 h. Obtained sodium titanate was washed with deionized water to remove excessive Na^+ ions and dried in an oven dryer for 24 h at 105 °C. After that, sodium titanate was calcined at 400 °C for 3 h. The obtained material was washed with water and ethanol and dried at 105 °C.

2.2.2. Synthesis of $\text{Ni}_3\text{S}_4/\text{Ag}_2\text{S}/\text{TiO}_2$ Nanocomposite

A thermal method was used for the synthesis of $\text{Ni}_3\text{S}_4/\text{Ag}_2\text{S}/\text{TiO}_2$. Initially, 1.51 g Na-TiO₂ (sodium titanate), 0.62 g NiCl_2 , and 0.27 g silver acetate were mixed in an agate mortar. Then, 1.2 g Na_2S was mixed and ground to get uniform powder reagents. A 3 mL amount of deionized was mixed with the prepared powdered reagents to get a black slurry, which was calcinated in a muffle furnace at 300 °C at the rate of 10 °C/min for 3 h. The powdered material was filtered, washed, and dried at 105 °C for the fabrication of $\text{Ni}_3\text{S}_4/\text{Ag}_2\text{S}/\text{TiO}_2/\text{CA}$ aerogel. A similar method was used to synthesize Ag_2S and Ni_3S_4 without TiO_2 .

2.2.3. Synthesis of $\text{Ni}_3\text{S}_4/\text{Ag}_2\text{S}/\text{TiO}_2/\text{Calcium Alginate Aerogel}$

Initially, 0.1 g $\text{Ni}_3\text{S}_4/\text{Ag}_2\text{S}/\text{TiO}_2$ was mixed with 4 mL water and stirred for 15 min to make a slurry in a 30 mL glass bottle. After that, 20 mL (2%) of sodium alginate was mixed dropwise with the $\text{Ni}_3\text{S}_4/\text{Ag}_2\text{S}/\text{TiO}_2$ slurry under continuous stirring to make a uniform solution. Then, 6 mL of CaCl_2 (3%) solution was added to the side wall of the bottle. This causes immediately formation of a gel-like structure, which was left for 3 h to solidify. The obtained $\text{Ni}_3\text{S}_4/\text{Ag}_2\text{S}/\text{TiO}_2/\text{calcium alginate}$ ($\text{Ni}_3\text{S}_4/\text{Ag}_2\text{S}/\text{TiO}_2/\text{CA}$) gel was thoroughly washed with deionized water to remove the excess CaCl_2 . The washed $\text{Ni}_3\text{S}_4/\text{Ag}_2\text{S}/\text{TiO}_2/\text{Alginate}$ gel was freeze-dried for 36 h at −55 °C in a freeze dryer. The $\text{Ni}_3\text{S}_4/\text{Ag}_2\text{S}/\text{TiO}_2/\text{CA}$ aerogel was washed with water and ethanol to remove the excessive reagents and dried at 80 °C for 24 h. A similar method was used to synthesize pure CA, $\text{Ag}_2\text{S}/\text{CA}$, and $\text{Ni}_3\text{S}_4/\text{CA}$ aerogels.

2.3. Adsorption Studies

The decontamination of OTC using the prepared materials was investigated in a batch mode by mixing 0.03 g of adsorbent in 30 mL OTC solution at a fixed pH and concentration. The optimum pH identification for OTC removal was studied between pH ranges from 2 to 10. The equilibrium concentration analysis was conducted at 50 mg/L OTC concentration at pH 6 for a 240 min reaction time. The equilibrium time analysis was performed at 5 mg/L and 50 mg/L OTC concentrations at pH 6 between 0 to 240 min. The adsorption capacity (q_t) of the aerogel materials was evaluated using the per unit mass of the adsorbent using the following equation:

$$q_t = \frac{(C_o - C_e)V}{W} \quad (1)$$

where C_o and C_e indicate the concentrations of OTC (mg L^{-1}) in the solution before and after its removal. The used volume of the OTC is denoted as V (L), and the used mass of the aerogel is represented as W (g).

2.4. Antimicrobial Studies

In this investigation, Ni₃S₄/CA, Ag/CA, TiO₂/CA, and Ni₃S₄/Ag₂S/TiO₂/CA aerogels were applied for antimicrobial purposes against the native microbial consortium present in the industrial beverage wastewater. Initially, the fresh wastewater sample was filtered through Whatman paper and serially diluted with ultrapure sterile water, inoculated in nutrient agar plates, submerged by a sterile glass spreader, and placed overnight into the incubator at 30 ± 2 °C temperature. After the incubation period on the cultured plates, microbial colonies were observed and counted with the help of a colony counter. These wastewater microbial consortia were saved as test organisms against the synthesized aerogels. These aerogels were directly applied to the diluted wastewater and placed on the magnetic stirrer in sunlight and inside the darkroom. The bacterial count was monitored at different time intervals monitored to measure the effect of the aerogel materials. For this purpose, 100 mL wastewater from each wastewater sample was divided into five 500 mL capacity flasks. An experiment was designed using the following: (i) only food industry wastewater (ii) food industry wastewater and Ni₃S₄/CA aerogel (iii) food industry wastewater and TiO₂/CA aerogel (iv) food industry wastewater and Ag₂S/CA aerogel and (v) food industry wastewater Ni₃S₄/Ag₂S/TiO₂/CA aerogel. All flasks were duplicated during the experiment, one series for dark incubation and another for sunlight incubation. The sunlight intensity and atmospheric temperature varied between 650 × 10² to 790 × 10² lux and 35 to 40 °C, respectively. The respective samples were exposed to 0 to 4 h of sunlight or incubated in a dark room simultaneously during the investigation. Subsequently, the turbidity of the solution and bacterial count was measured. In parallel, the antimicrobial potential of synthesized aerogels was analyzed from the microbial consortia obtained from the wastewater sample of food industry sites.

2.4.1. MIC/MBC Values of Aerogels

The antimicrobial potential of synthesized aerogel materials is important because of their potential application and suitability for antiseptic use. The minimum inhibitory concentration (MIC) and minimum bactericidal concentration (MBC) values were determined to investigate the antimicrobial potential of the aerogel material. The MIC is the least amount of aerogel material that prevents the cell formation or the visible growth of bacteria or that acts as bacteriostatic in growth media or solution. The lowest level or concentration of aerogel materials that significantly inhibits the microbial growth is known as the MIC. A minimum dose or concentration of material that causes the death of the microbial population is known as MBC. The MIC and MBC of hybrid aerogels against the indigenous or natural microbial consortia obtained during the microbial count were performed using the broth dilution method previously recommended by the Clinical and Laboratory Standards Institute. The bacterial culture from the food water industries was optimized in Muller Hinton Broth media and set at 0.5 turbidity according to the McFarland standard, indicating a microbial population 1 – 5 × 10⁶ CFU/mL in 0.1 mL solution. The aerogel materials were crushed as a fine powder and suspended at 0, 2, 4, 8, 16, 32, 64, 128, 256, and 512 µg/mL in 50 µL of the broth, and with an equal volume of 50 µL of bacterial culture were placed in wells of on a 96 wells plate. The tetracycline antibiotic was used as a positive control in separate wells of the same plate which was then incubated at 35 °C overnight.

2.4.2. Bacterial Zone Inhibition Analysis

Bacterial zone inhibition was conducted using antimicrobial aerogels on the Petri plate solid agar media, also known as the Kirby–Bauer test. This assay is rapid and inexpensive for testing the antimicrobial activity of aerogels. Zone inhibition assay is a qualitative antimicrobial test for antibiotics, chemical compounds, medical fabrics, and other materials used in medical device manufacturing. Previously obtained bacterial culture from the wastewater were purified, and then spread 0.1 mL on the surface of cold agar media plates with the help of a sterile glass rod spreader. The aerogel's 100 µg were applied to the center

of the Petri plate surface. The dish was placed in the incubator for 24 h; during this period, the compound diffuses into the surroundings, preventing bacterial growth around the compound, and creating a zone of inhibition. The size of the zone of inhibition is related to the antimicrobial property of the applied aerogels.

2.5. Characterization

The surface morphological studies, elemental analysis, and mapping were carried out through field emission scanning electron microscopy (JEOL, JSM-7600F, FESEM, Tokyo, Japan). The crystallinity and phases of as-prepared samples were analysed by X-ray powder diffractometer (Rigaku, Ultima IV XRD, Tokyo, Japan). The X-ray photoelectron spectroscopy (XPS; ESCALAB 250, Thermo Fisher Scientific, Oxford, UK; used at a monochromatized Al K α X-ray source $\lambda \frac{1}{4}$ 1486.6 eV) was used to detect functional groups and their interactions in the Ni₃S₄/Ag₂S/TiO₂/CA aerogel. Photoluminescence (RF-5301PC Shimadzu, Kyoto, Japan, spectro-fluorophotometer) and absorbance spectra (UV-visible spectrophotometer; PerkinElmer 750, Waltham, MA, USA) measurements were performed to study the charge recombination and band gap of Ni₃S₄/Ag₂S/TiO₂/CA aerogel.

3. Results and Discussion

3.1. Synthesis and Characterization

Generally, pure TiO₂ is a crystalline material with a smooth surface. After treatment with the concentrated NaOH, a mixed phase, like rutile or anatase, and sodium titanate are formed. The mixed phase is generally amorphous with a lamellar structure and defects, providing the surface area to bind with the other semiconductor materials. Moreover, Na⁺ is ion-exchangeable in sodium titanate, which can help in the adsorption or synthesis of new materials using their ion-exchange properties [13,14]. Herein, Ni²⁺ and Ag⁺ ions may replace the Na⁺ ions and form more stable sulfides on the surface of the TiO₂. A schematic diagram for synthesizing the Ni₃S₄/Ag₂S/TiO₂/CA aerogel is shown in Figure 1. Several instrumental techniques such as SEM, EDX, elemental mapping, XRD, XPS, etc. have been used to characterize the synthesized materials.

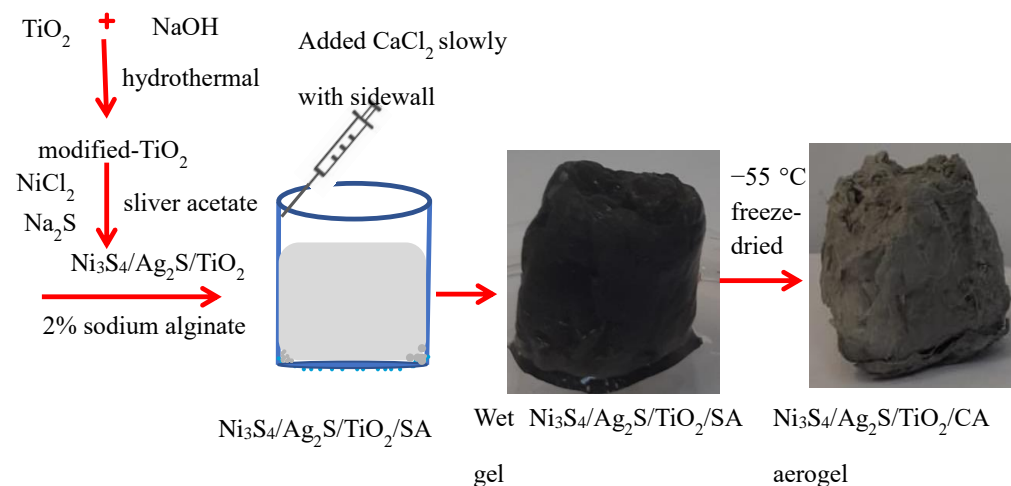


Figure 1. Schematic diagram representing the synthesis of Ni₃S₄Ag₂S/TiO₂/CA aerogel. The SEM images of Ni₃S₄, Ag₂S and TiO₂ particles can get an idea of their individual sizes (Figure S1). The SEM images of TiO₂ show aggregated clusters of nano-ranged particles. Furthermore, the TEM of TiO₂ shows that nano-ranged particles (<100 nm) are aggregated into clusters of ~500 nm size. The SEM of Ag₂S shows the majority of particles of sizes in the range of 20–100 nm along with the observance of small clusters of particles with even larger sizes. The SEM of Ni₃S₄ shows interconnected globules of micrometer size; however, small clusters of loosely packed particles (approximately in the nanometers range) can be seen protruding out of the globules.

The morphology of the films was studied by SEM as presented in Figure 2. Pure CA shows a continuous uneven, porous surface with the observance of bulges and small craters. The cross-section seems compact, and the thickness is in the range of 1–1.5 μm . In the case of $\text{Ni}_3\text{S}_4/\text{CA}$ (d–f), $\text{Ag}_2\text{S}/\text{CA}$ (g–i), and $\text{Ni}_3\text{S}_4/\text{Ag}_2\text{S}/\text{TiO}_2/\text{CA}$ (j–l) the surfaces are relatively much rougher and porous due to the embedded Ni_3S_4 , Ag_2S or $\text{Ni}_3\text{S}_4/\text{Ag}_2\text{S}/\text{TiO}_2$. In $\text{Ni}_3\text{S}_4/\text{Ag}_2\text{S}/\text{TiO}_2/\text{CA}$, the $\text{Ni}_3\text{S}_4/\text{Ag}_2\text{S}/\text{TiO}_2$ aggregates can be seen protruding out of the CA strands. It can be assumed that Ni_3S_4 , Ag_2S , or $\text{Ni}_3\text{S}_4/\text{Ag}_2\text{S}/\text{TiO}_2$, apart from covering the surface, is also deeply embedded inside the CA network with Ni_3S_4 , Ag_2S or $\text{Ni}_3\text{S}_4/\text{Ag}_2\text{S}/\text{TiO}_2$ aggregates protruding out from inside. In contrast to CA, the rougher morphology of $\text{Ni}_3\text{S}_4/\text{Ag}_2\text{S}/\text{TiO}_2/\text{CA}$ might be due to the nucleation effect of embedded, protruding or surface-covered nanomaterials, which creates depressions or ruptured sites in the CA. The EDAX analysis of $\text{Ni}_3\text{S}_4/\text{Ag}_2\text{S}/\text{TiO}_2/\text{CA}$ shows the presence of C, O, Ti, Ni, Ag, S and Ca. The non-observance of Na and subsequent presence of Ca suggests successful replacement of Na with Ca during the CaCl_2 reaction with $\text{Ni}_3\text{S}_4/\text{Ag}_2\text{S}/\text{TiO}_2/\text{SA}$ (Figure 3). The uniform distribution of C, O, Ti, Ni, Ag, S and Ca in the elemental mapping analysis also suggests the efficacy of the synthesis methodology (Figure 4).

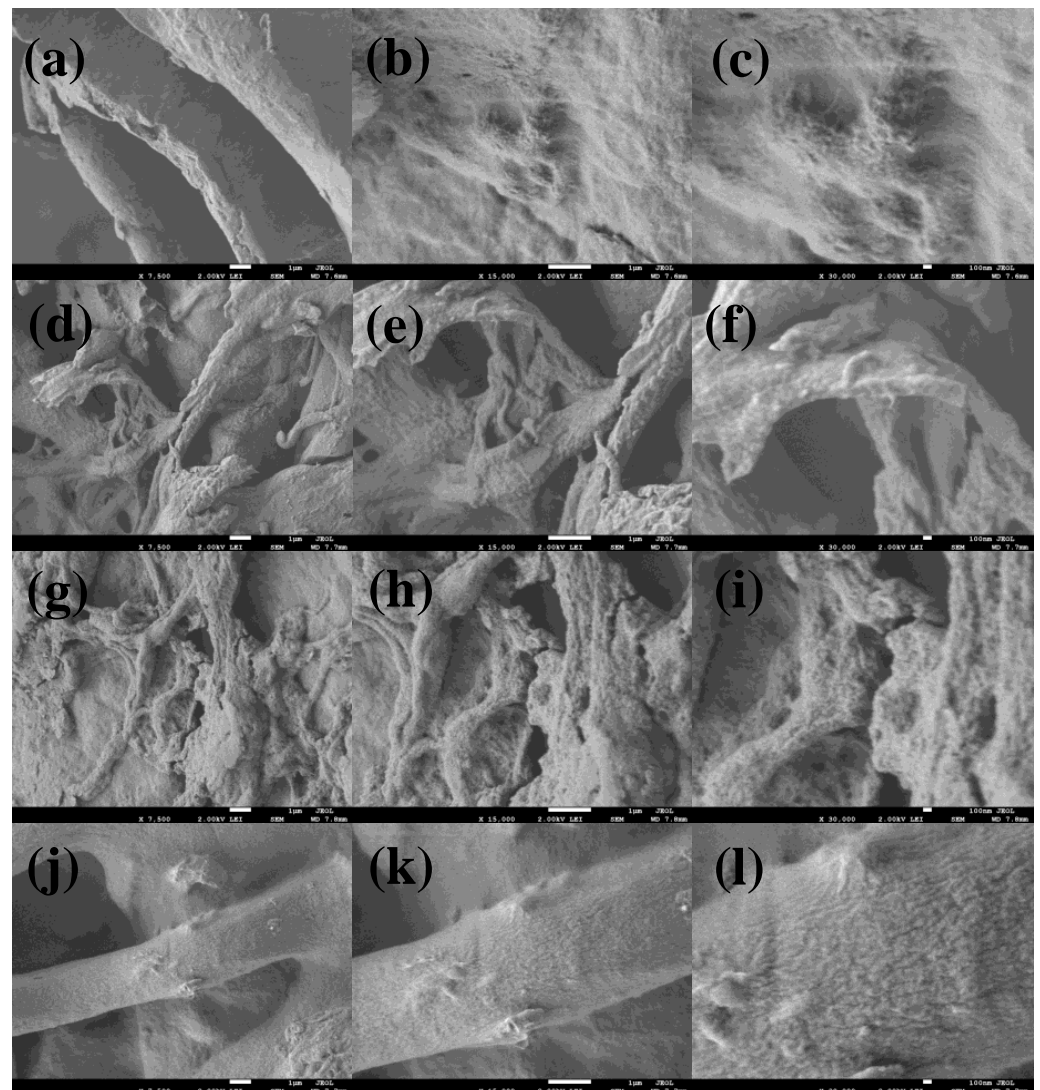


Figure 2. SEM images of CA (a–c), $\text{Ni}_3\text{S}_4/\text{CA}$ (d–f), $\text{Ag}_2\text{S}/\text{CA}$ (g–i) and $\text{Ni}_3\text{S}_4/\text{Ag}_2\text{S}/\text{TiO}_2/\text{CA}$ (j–l) at different magnifications.

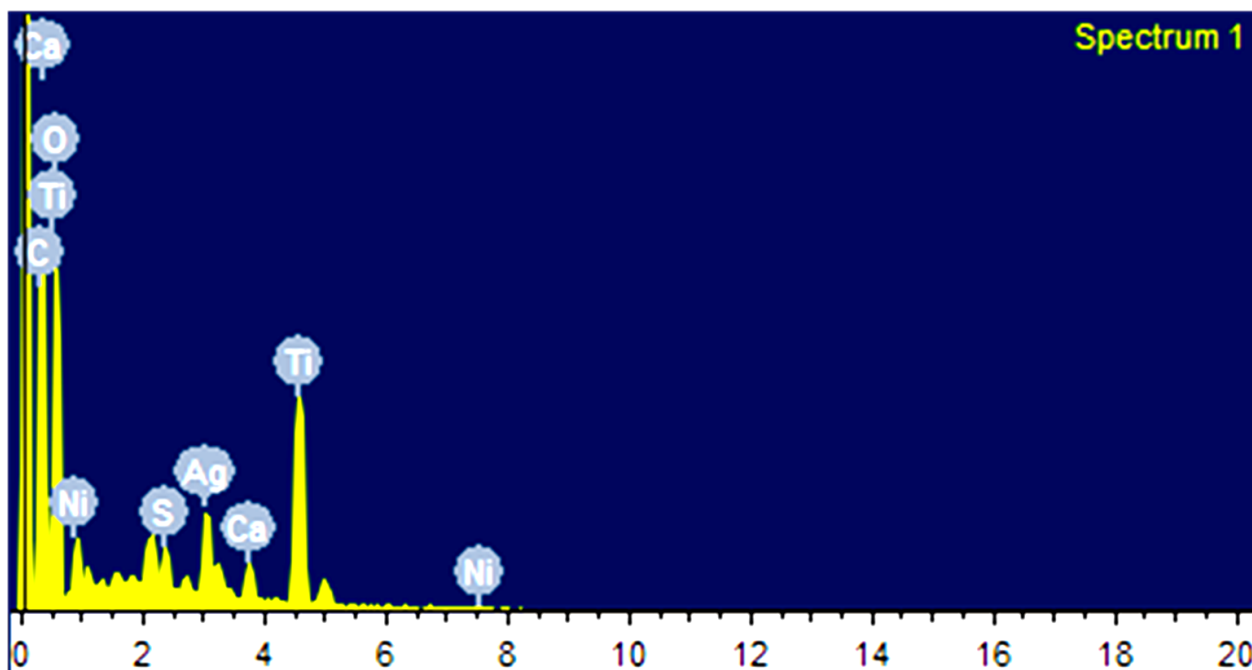


Figure 3. EDAX analysis of $\text{Ni}_3\text{S}_4\text{Ag}_2\text{S}/\text{TiO}_2/\text{CA}$.

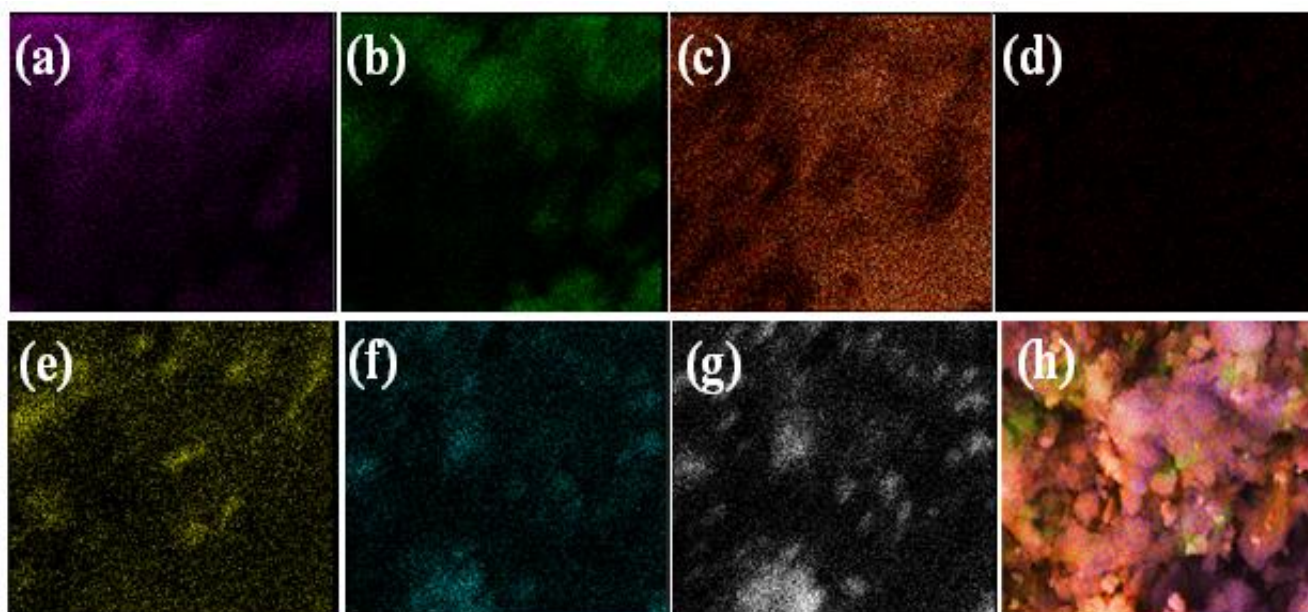


Figure 4. Elemental mapping $\text{Ni}_3\text{S}_4/\text{Ag}_2\text{S}/\text{TiO}_2/\text{CA}$. Carbon (a), oxygen (b), Titanium (c), Nickel (d), Ca (e), Sulfur (f), Ag (g) and mixed elemental mapping of all elements (h).

The XRD pattern of CA, $\text{Ni}_3\text{S}_4/\text{CA}$, $\text{Ag}_2\text{S}/\text{CA}$ and $\text{Ni}_3\text{S}_4/\text{Ag}_2\text{S}/\text{TiO}_2/\text{CA}$ are presented in Figure 5. All the samples showed a broad peak in the region of $\sim 20^\circ 2\theta$ owing to the presence of amorphous CA and the peaks of Ni_3S_4 , Ag_2S , and TiO_2 are not distinctly observed. Similar reports of highly diffused peaks of fillers in the polymer matrix have been previously reported [14].

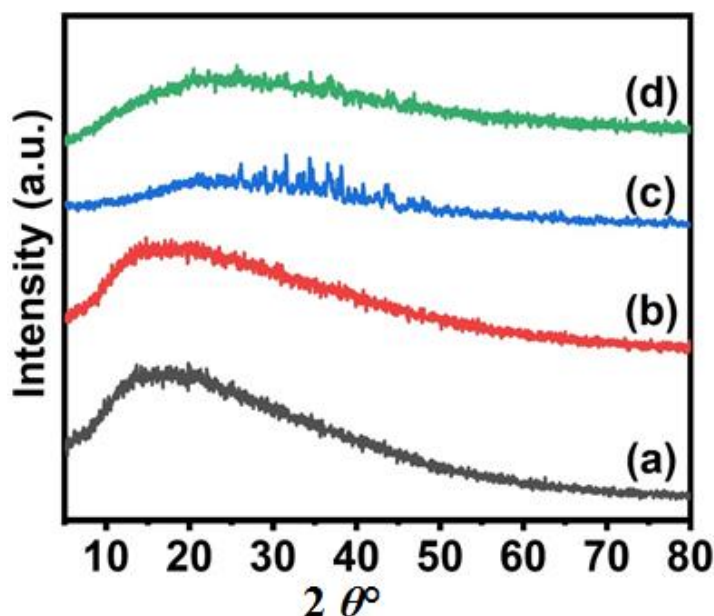


Figure 5. XRD patterns of CA (a), $\text{Ni}_3\text{S}_4/\text{CA}$ (b), $\text{Ag}_2\text{S}/\text{CA}$ (c), and $\text{Ni}_3\text{S}_4/\text{Ag}_2\text{S}/\text{TiO}_2/\text{CA}$ (d).

The PL emission spectra of CA, $\text{Ni}_3\text{S}_4/\text{CA}$, $\text{Ag}_2\text{S}/\text{CA}$, and $\text{Ni}_3\text{S}_4/\text{Ag}_2\text{S}/\text{TiO}_2/\text{CA}$ are presented in Figure 6. The PL spectra are indicative of the charge separation rate and migration efficiency of the charge carriers. The decrease in the PL intensity of $\text{Ni}_3\text{S}_4/\text{CA}$ and $\text{Ag}_2\text{S}/\text{CA}$ compared to CA and a further decrease in loading with Ni_3S_4 , Ag_2S and TiO_2 suggest the highest photocatalytic activity of $\text{Ni}_3\text{S}_4/\text{Ag}_2\text{S}/\text{TiO}_2/\text{CA}$. The excitation wavelength of $\text{Ni}_3\text{S}_4/\text{Ag}_2\text{S}/\text{TiO}_2/\text{CA}$ falls in the visible light region, thereby indicating its visible light activity. The peaks in the region 450–500 nm are related to charge recombination from the conduction band to the recombination center at the ground state. Thus, the lowest intensity peak of $\text{Ni}_3\text{S}_4/\text{Ag}_2\text{S}/\text{TiO}_2/\text{CA}$ suggests its lowest charge recombination and hence the longer lifetime of the photogenerated carrier [15].

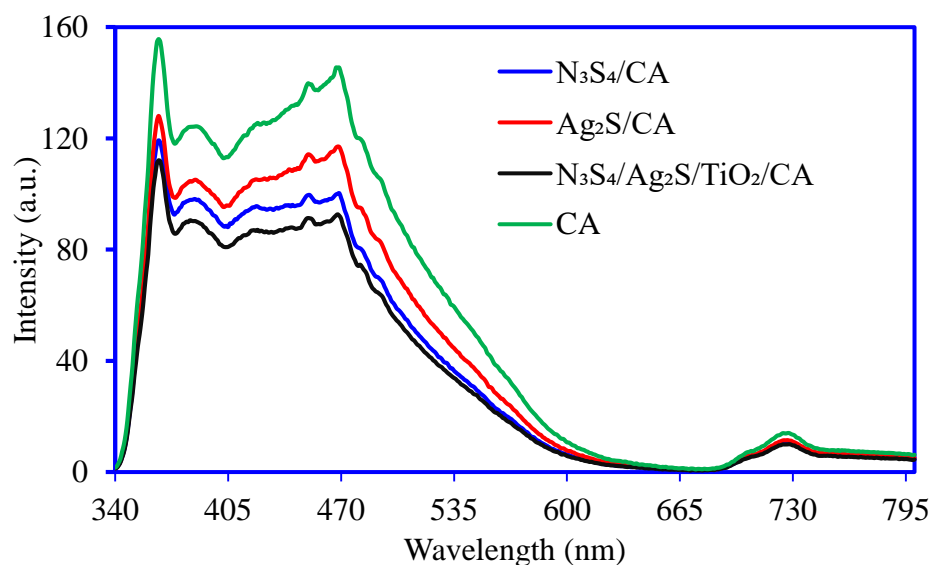


Figure 6. PL emission spectra of CA, $\text{Ni}_3\text{S}_4/\text{CA}$, $\text{Ag}_2\text{S}/\text{CA}$, and $\text{Ni}_3\text{S}_4/\text{Ag}_2\text{S}/\text{TiO}_2/\text{CA}$.

The elemental composition of $\text{Ni}_3\text{S}_4/\text{Ag}_2\text{S}/\text{TiO}_2/\text{CA}$ studied by XPS as presented in Figure 7 showed the presence of C1s, O1s, Ti2p, Ni2p, Ag3d, Ca2p and S2p peaks corresponding to the presence of oxygen (48.1%), carbon (38.1%), titanium (7.6%), calcium (2.6%), nickel (2.4%), silver (0.9%), and sulfur (0.3%). The C1s spectra can be deconvoluted into

283.80, 284.95 and 288.88 eV peaks corresponding to the C–O–Ti, C=C & C–C, and O–C=O, which correspond to the functionality of the alginate ring and its interaction with Ti and water molecules, respectively [16]. The high percentage of C–C and C–O peaks compared to COOH is due to the major carbon skeleton in rings, C–O in rings, and interconnections between rings and the carbon bonded to the hydroxyl group. The O1s spectra consist of three peaks at 529.07, 531.21 and 532.88 eV corresponding to the oxygen of Ti–O bonds in TiO₂ (O²⁻ from TiO₂), C–O and associated water molecules, respectively [17–19]. The Ti 2p_{3/2} and Ti 2p_{1/2} peaks at 459.42 and 465.68 eV are due to the presence of TiO₂ [20]. The presence of Ni₃S₄ is confirmed by the Ni 2p_{3/2} peak at 854.69, 2p_{1/2} at 873.4 eV and two shakeup satellite peaks [21,22]. The peaks at 367.88 and 372.34 eV are assigned to Ag 3d_{5/2} and Ag 3d_{3/2} of Ag⁺ ions in Ag₂S, respectively, while the S p_{1/2} and S p_{3/2} located at 162.4 and 161.2 eV, respectively, are due to the S of both sulfides [23]. The presence of Ca2p peaks around 360 eV in the survey scan, and subsequently, no observation of Na, confirms the successful replacement of Na by Ca during the composite reaction with CaCl₂ aqueous solution.

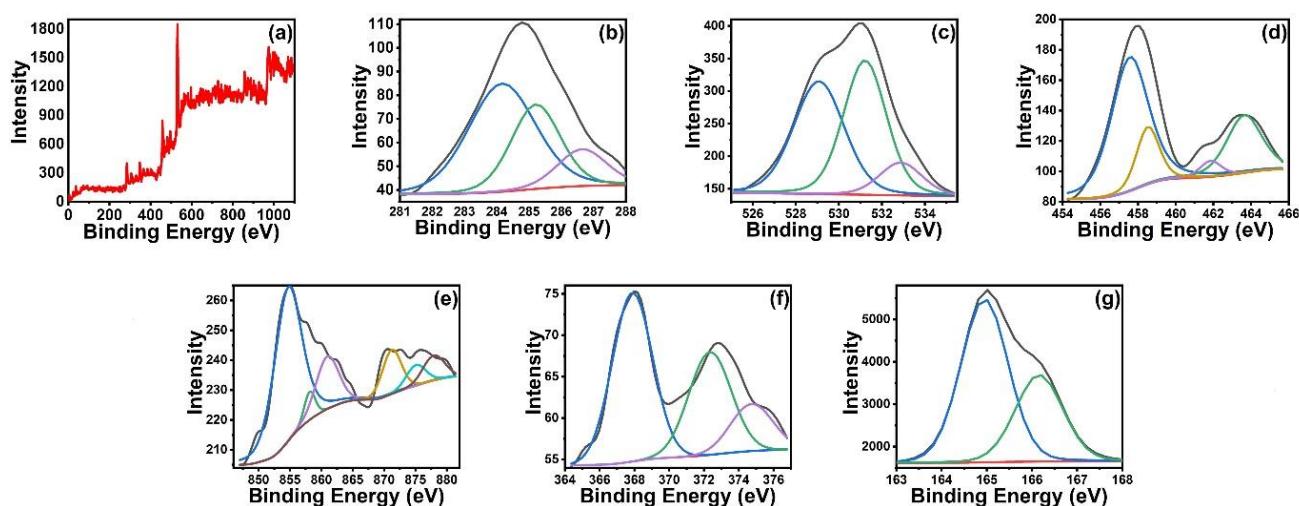


Figure 7. XPS spectra of Ni₃S₄/Ag₂S/TiO₂/CA. Survey scan (a), C1s (b), O1s (c), Ti2p (d), Ni2p (e), Ag3d (f) and S2p (g).

3.2. OTC Removal Studies

The adsorption efficacies of the synthesized aerogels for the removal of the OTC have been evaluated at 10 and 50 mg/L concentrations, and the results are depicted in Figure 8. The OTC adsorption results revealed that the removal capacity of the aerogel increases with the increase in the functionality of the adsorbent. The adsorption capacity of the prepared aerogels is in the following order: Ni₃S₄/Ag₂S/TiO₂/CA > Ni₃S₄/CA > TiO₂/CA > Ag₂S/CA > CA. These results revealed that Ni₃S₄/Ag₂S/TiO₂/CA is the best adsorbent for removing the OTC due to the presence of large functional groups on the surface. Therefore, Ni₃S₄/Ag₂S/TiO₂/CA aerogel was selected for the brief adsorption studies to identify the optimum experimental condition for OTC removal.

The adsorption of OTC onto Ni₃S₄/Ag₂S/TiO₂/CA aerogel was investigated at pH ranges from 2 to 10; the results are depicted in Figure 9. The results revealed that solution pH affects the OTC adsorption onto Ni₃S₄/Ag₂S/TiO₂/CA aerogel, with optimum absorption at pH 6. The optimum adsorption at pH 6 can be explained on the basis of the pK_a of OTC. In an acidic medium, OTC is positively charged (OTC⁺) while zwitterionic (OTC[±]) forms in a neutral medium, and the negatively charged molecular form (OTC⁻) is found in a basic medium [24,25]. The pK_a values of the OTC ionic forms are 3.57, 7.49, and 9.88. Under the acidic condition (at pH 3), the majority of OTC molecules (80%) exist in the form of cationic (OTC⁺) molecules, which show electrostatic repulsion with the protonated Ni₃S₄/Ag₂S/TiO₂/CA aerogel. As the solution pH is increased to 6, all the OTC molecules exist in zwitterionic (OTC[±]) form, and the surface charge of the aerogel is

close to neutral. The formation of H-bonding and $n-\pi$ electron donor-acceptor interaction is possible to a more considerable extent due to the presence of the double bond benzene ring, oxygen and nitrogen, sulfur-containing functional groups on OTC molecules and $\text{Ni}_3\text{S}_4/\text{Ag}_2\text{S}/\text{TiO}_2/\text{CA}$ aerogel [10,26]. Under alkaline conditions, the monovalent and divalent OTC anions become more prominent in the solution, showing an electrostatic repulsion with the deprotonated $\text{Ni}_3\text{S}_4/\text{Ag}_2\text{S}/\text{TiO}_2/\text{CA}$ aerogel surface, resulting a reduction in the adsorption capacity [27].

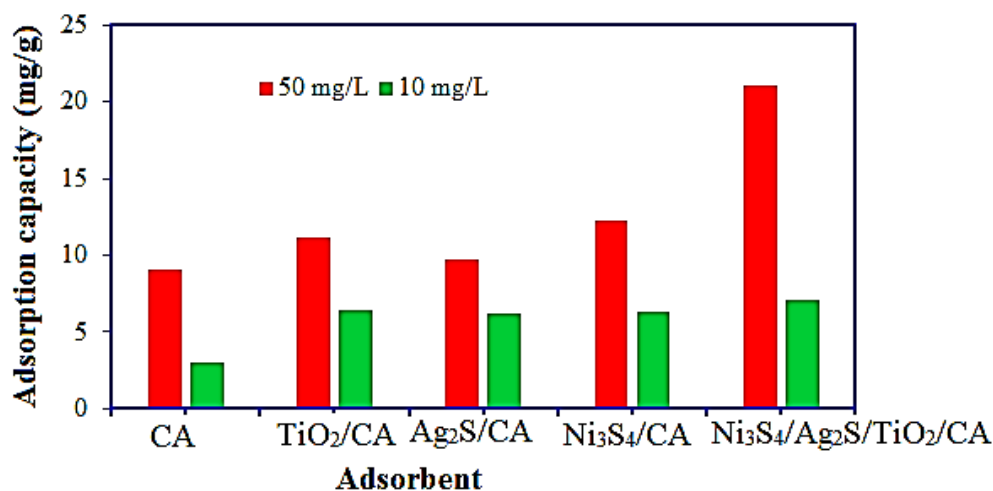


Figure 8. Comparison of the adsorption efficiencies of synthesized aerogels for the removal of OTC. (aerogel mass: 0.03 g, OTC volume: 30 mL, time: 180 min, pH: 6).

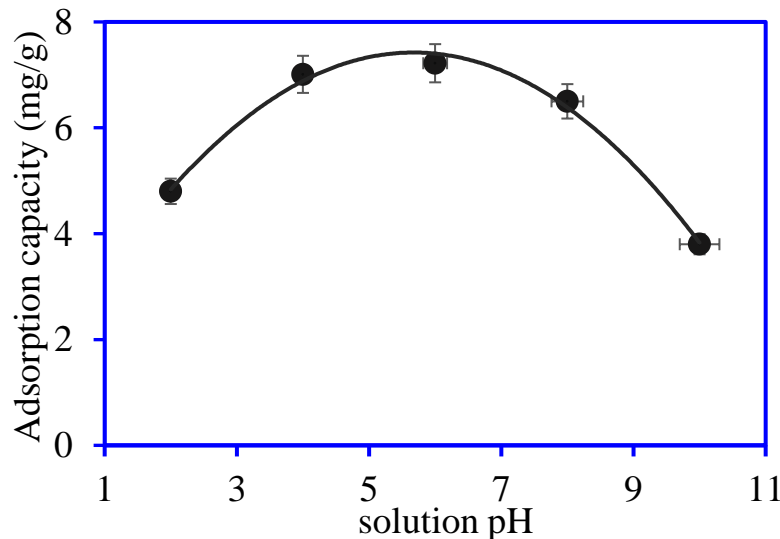


Figure 9. Plot for OTC adsorption at different solution pH onto $\text{Ni}_3\text{S}_4/\text{Ag}_2\text{S}/\text{TiO}_2/\text{CA}$ aerogel. (OTC conc.: 10 mg/L, aerogel mass: 0.03 g, OTC volume: 30 mL, time: 180 min).

The adsorption isotherm studies of OTC onto $\text{Ni}_3\text{S}_4/\text{Ag}_2\text{S}/\text{TiO}_2/\text{CA}$ were investigated at varying initial concentrations between 5 mg/L to 50 mg/L, as shown in Figure 10. The OTC adsorption rate increases with the increase in the OTC molecules in the solution from 5 mg/L to 30 mg/L. A saturation of $\text{Ni}_3\text{S}_4/\text{Ag}_2\text{S}/\text{TiO}_2/\text{CA}$ active sites has been observed beyond 30 mg/L, meaning that equilibrium between OTC and $\text{Ni}_3\text{S}_4/\text{Ag}_2\text{S}/\text{TiO}_2/\text{CA}$ has been established. At lower concentrations, OTC molecules are present in fewer numbers, and many active sites on $\text{Ni}_3\text{S}_4/\text{Ag}_2\text{S}/\text{TiO}_2/\text{CA}$ are available for adsorption. As the ratio between OTC molecules and active sites reduces, $\text{Ni}_3\text{S}_4/\text{Ag}_2\text{S}/\text{TiO}_2/\text{CA}$ surface sites reach equilibrium [28].

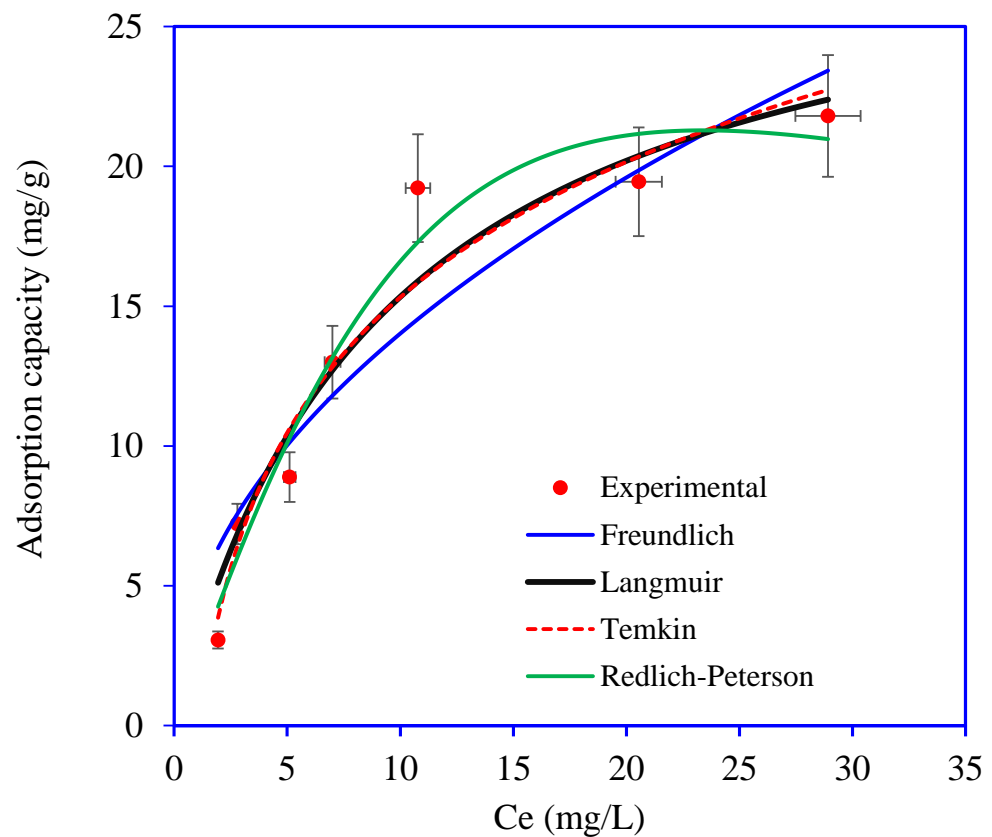


Figure 10. Plot for OTC adsorption isotherms onto $\text{Ni}_3\text{S}_4/\text{Ag}_2\text{S}/\text{TiO}_2/\text{CA}$ aerogel. (aerogel mass: 0.03 g, OTC volume: 30 mL, time: 180 min, pH: 6).

The relationship concerning the $\text{Ni}_3\text{S}_4/\text{Ag}_2\text{S}/\text{TiO}_2/\text{CA}$ capacity and OTC loading concentration can be discovered by fitting the experimental equilibrium data to Langmuir, Freundlich, Temkin, and Redlich–Peterson isotherm models. The nonlinear equations for the Langmuir, Freundlich, Temkin, and Redlich–Peterson isotherm are as follows:

$$\text{Langmuir : } q_e = \frac{q_m k_L C_e}{1 + k_L C_e} \quad (2)$$

$$\text{Freundlich : } q_e = k_F C_e^{\frac{1}{n}} \quad (3)$$

$$\text{Temkin : } q_e = B_t \ln(K_t C_e) \quad (4)$$

$$\text{Redlich–Peterson : } q_e = \frac{K_{RP} C_e}{1 + \alpha_{RP} C_e^\beta} \quad (5)$$

where, C_e : equilibrium concentration, q_e : equilibrium capacity, q_m : monolayer adsorption capacity, k_F and, $1/n$: Freundlich constant related to adsorption intensity and adsorption capacity, K_t : equilibrium binding constant, and B_t : the heat of adsorption, K_{RP} (L/g) and α_{RP} : Redlich–Peterson isotherm constants and β : exponent reflect the heterogeneity of the aerogels. The values of the OTC adsorption isotherm parameters are incorporated in Table 1. The isotherm parameters and error function values are obtained from the plots shown in Figure 10. Based on the lower error functions RMSD, χ^2 values, and higher R^2 value, the Redlich–Peterson isotherm model is most suited to the OTC adsorption data onto $\text{Ni}_3\text{S}_4/\text{Ag}_2\text{S}/\text{TiO}_2/\text{CA}$. These isotherm modeling results demonstrate that adsorption of OTC occurred on the heterogeneous surface of the $\text{Ni}_3\text{S}_4/\text{Ag}_2\text{S}/\text{TiO}_2/\text{CA}$. The Redlich–Peterson isotherm model is the combined model of the Langmuir and Freundlich model. Therefore, OTC adsorption onto $\text{Ni}_3\text{S}_4/\text{Ag}_2\text{S}/\text{TiO}_2/\text{CA}$ has the characteristics of the Langmuir and Freundlich model.

Table 1. The values of adsorption kinetics parameters for OTC onto Ni₃S₄/Ag₂S/TiO₂/CA aerogel.

Kinetic Model	Parameters	10 mg/L	50 mg/L
Pseudo-first order:	q_e (exp) (mg g ⁻¹):	7.1	21
	q_e (cal) (mg g ⁻¹):	7.074	21.043
	k_1 (min ⁻¹):	0.0266	0.022
	R ² :	0.939	0.983
	RMSE:	0.437	0.651
	χ^2	1.469	0.412
Pseudo-second order:	q_e (cal) (mg g ⁻¹):	8.216	25.454
	k_2 (g mg ⁻¹ min ⁻¹):	0.0042	0.0010
	R ² :	0.934	0.991
	RMSE:	0.385	0.454
	χ^2	0.629	0.091
Elovich model:	a (mg g ⁻¹ min ⁻¹):	0.635	1.054
	β (mg g ⁻¹):	0.587	0.163
	R ² :	0.944	0.993
	RMSE:	0.353	0.691
	χ^2	0.219	0.339

The OTC adsorption rate onto Ni₃S₄/Ag₂S/TiO₂/CA as a function of adsorption time was investigated at 10 mg/L and 50 mg/L concentrations. Figure 11 shows the kinetic plot for the OTC adsorption onto Ni₃S₄/Ag₂S/TiO₂/CA. Initially, OTC was adsorbed rapidly at 10 mg/L concentration, and equilibrium was attained within 60 min due to the large number of vacant sites on the Ni₃S₄/Ag₂S/TiO₂/CA, while at 50 mg/L concentration, equilibrium was attained within 150 min. Beyond 150 min, adsorption became slower due to the active sites' saturation [29].

Moreover, to find the rate of OTC removal by Ni₃S₄/Ag₂S/TiO₂/CA, the kinetic data were applied to the pseudo-first order, pseudo-second order, and Elovich models. The non-linear equations of pseudo-first order, pseudo-second order, and Elovich models are as follows:

$$\text{Pseudo – first order : } q_t = q_e \left(1 - e^{(-k_1 t)} \right) \quad (6)$$

$$\text{Pseudo – second order : } q_t = \frac{q_e^2 k_2 t}{[k_2 (q_e) t + 1]} \quad (7)$$

$$\text{Elovich models : } q_t = \frac{1}{\beta} \ln(\alpha \beta t) \quad (8)$$

where, q_e and q_t are adsorption capacities at equilibrium and at time t (min), k_1 is the pseudo-first order rate constant, k_2 is the pseudo-second order rate constant, α and β are adsorption and desorption rate constants for the Elovich model. The plots for the pseudo-first order, pseudo-second order, and Elovich models are included in Figure 11 and the data obtained from the respective plots are depicted in Table 2. Based on higher R² values, lower chi-square (χ^2), and root-mean-square deviation (RMSD), the Elovich model is the best model for explaining the adsorption of OTC onto Ni₃S₄/Ag₂S/TiO₂/CA at both concentrations. The Elovich model's fitting ascribes the OTC adsorption onto Ni₃S₄/Ag₂S/TiO₂/CA to chemisorption [24,30]. These results reveal that the OTC adsorption rate onto Ni₃S₄/Ag₂S/TiO₂/CA decreases exponentially with the increase in the OTC amount on the aerogel's heterogeneous surface [31].

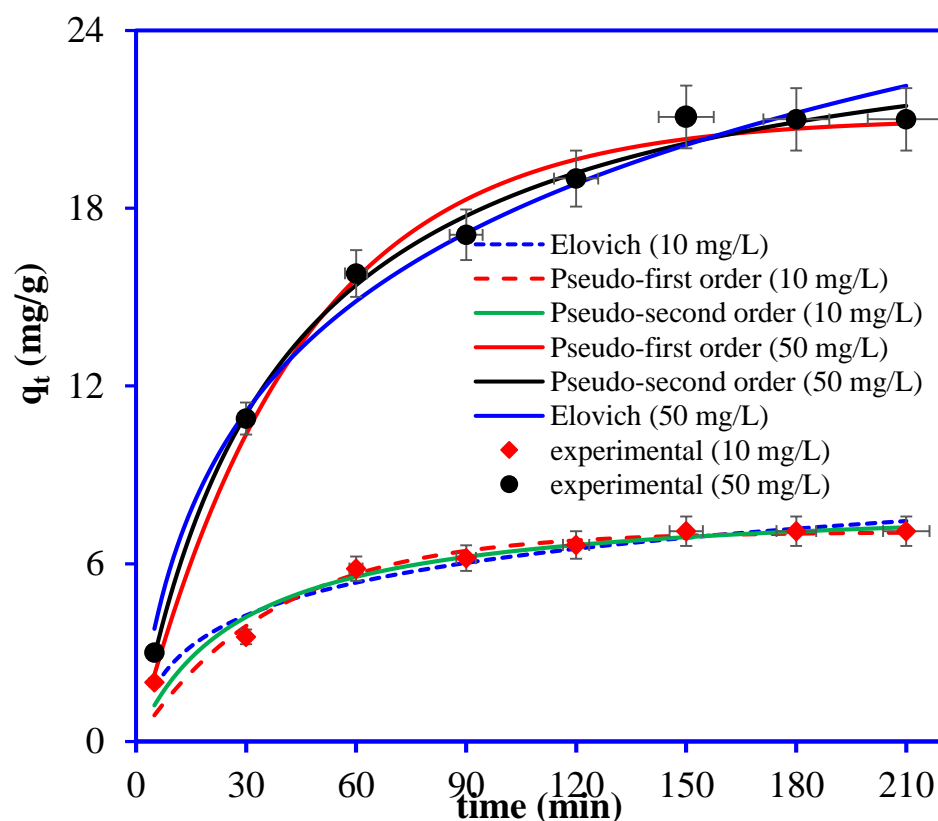


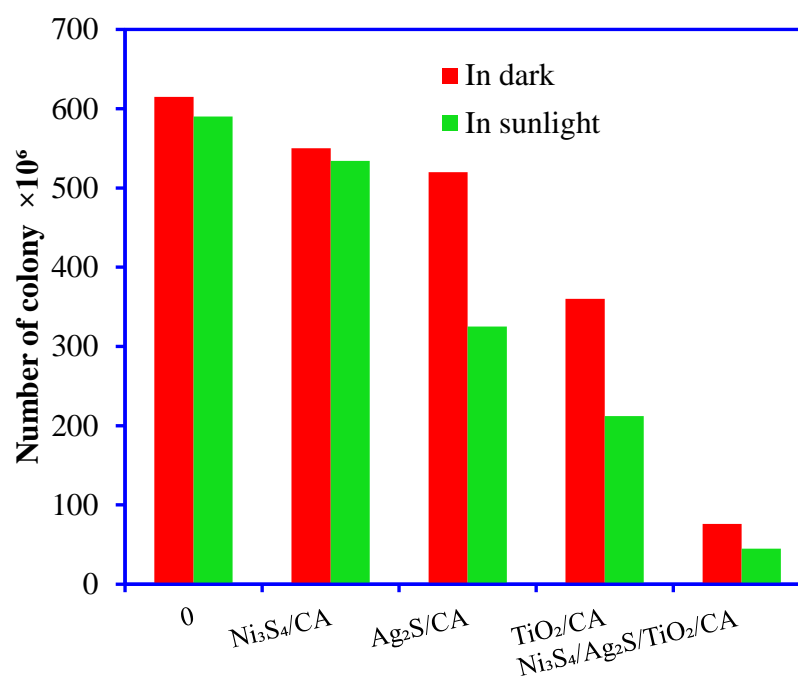
Figure 11. Plot for OTC adsorption kinetics onto $\text{Ni}_3\text{S}_4/\text{Ag}_2\text{S}/\text{TiO}_2/\text{CA}$ aerogel. (OTC conc.: 50 mg/L, aerogel mass: 0.03 g, OTC volume: 30 mL, time: 180 min, pH: 6).

3.3. Antimicrobial Studies

This study used $\text{Ni}_3\text{S}_4/\text{CA}$, $\text{Ag}_2\text{S}/\text{CA}$, TiO_2/CA , and $\text{Ni}_3\text{S}_4/\text{Ag}_2\text{S}/\text{TiO}_2/\text{CA}$ aerogels as chemical agents against the bacterial consortium obtained from the industrial beverage wastewater. Initially, the maximum bacterial count was 6.15×10^6 on the plate after the incubation overnight in optimum conditions in the incubator. Further, these microbial consortia were saved as test organisms against the synthesized aerogels. The tested aerogel materials significantly influenced bacterial growth in the absence and presence of sunlight incubation because sunlight activates the aerogels with high electron transportation in the system. After 4 h incubation in sunlight, the test compound led to a maximum decline in colony formation up to 4.5×10^5 in the presence of $100 \mu\text{g}/\text{mL}$ $\text{Ni}_3\text{S}_4/\text{Ag}_2\text{S}/\text{TiO}_2/\text{CA}$ aerogels in the batch incubation system (Figure 12). Further, the $\text{Ni}_3\text{S}_4/\text{Ag}_2\text{S}/\text{TiO}_2/\text{CA}$ aerogel was incubated hour-wise with native bacteria in sunlight and dark conditions (Figure 13). Four-hour incubation with aerogel in sunlight led to a complete decline in the bacterial growth. The higher activity of the synthesized aerogels in solar light can be explained on the basis of the photocatalytic activity of the semiconductor materials in the aerogel materials. The semiconductors Ni_3S_4 , Ag_2S , TiO_2 in their respective aerogels can be easily activated by solar light photons, which produce the electron-hole pairs, which react with the surface oxygen and water molecules and produce $^-\text{O}_2$, and OH radicals on the surface of the aerogel. These $^-\text{O}_2$, and OH radicals absorbed by the bacterial cell, break the cell wall, release the nucleic acid, and damage the microbial DNA, resulting in the cell's death [32].

Table 2. The values of adsorption isotherm parameters for OTC onto Ni₃S₄/Ag₂S/TiO₂/CA aerogel.

Isotherm Model	Parameters	Values
Langmuir	q_m (mg g ⁻¹):	29.571
	K_L (L mg ⁻¹):	0.107
	R^2 :	0.9370
	RMSE:	1.660
	χ^2 :	1.852
Freundlich	n:	2.069
	K_f (mg g ⁻¹) (mg L ⁻¹) ^{-1/n_F} :	4.609
	R^2 :	0.8739
	RMSE:	2.349
	χ^2 :	3.622
Temkin	B_t (J mg ⁻¹):	553.70
	K_t (L mg ⁻¹):	0.895
	R^2 :	0.9431
	RMSE:	1.577
	χ^2 :	1.354
Redlich–Peterson	K_{RP} (L/g):	2.242
	$\alpha_{RP} \times 10^{-3}$ (L/mg):	7.309
	β :	1.681
	R^2 :	0.9602
	RMSE:	1.319
	χ^2 :	1.154

**Figure 12.** Microbial decontamination properties of Ni₃S₄/CA, Ag₂S/CA, TiO₂/CA, and Ni₃S₄/Ag₂S/TiO₂/CA aerogels against the native microbial culture in the absence and presence of sunlight (aerogel dose 100 µg/mL).

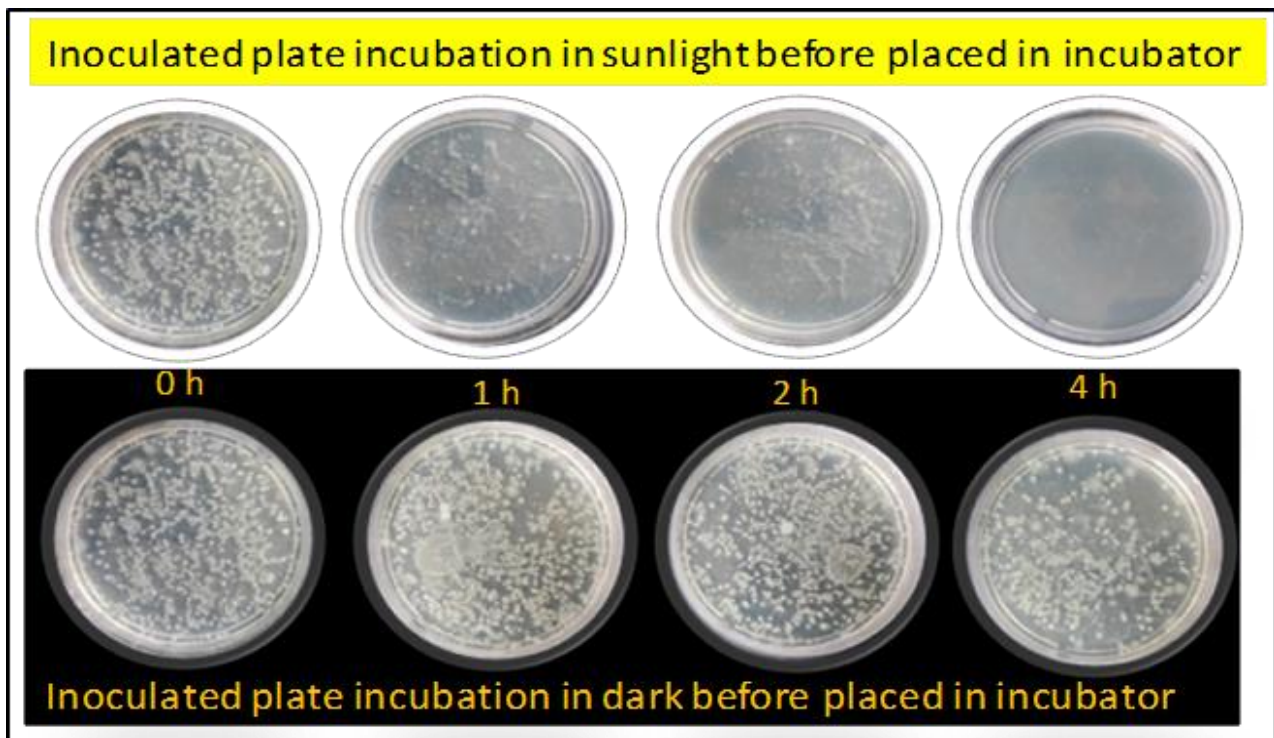


Figure 13. Bacterial growth control properties of $\text{Ni}_3\text{S}_4/\text{Ag}_2\text{S}/\text{TiO}_2/\text{CA}$ aerogel at different time intervals of 0–4 h in the absence and presence of sunlight (aerogel dose $100 \mu\text{g}/\text{mL}$).

3.3.1. Bacterial Zone Inhibition

Zone inhibition assay reflects the antimicrobial behavior of $\text{Ni}_3\text{S}_4/\text{CA}$, $\text{Ag}_2\text{S}/\text{CA}$, TiO_2/CA , and $\text{Ni}_3\text{S}_4/\text{Ag}_2\text{S}/\text{TiO}_2/\text{CA}$ aerogels which may be used for medical fabrics and device manufacturing in future. The bacterial culture from the wastewater was spread on the surface of solid agar media plates; $100 \mu\text{g}$ of each aerogel was applied to the center of a separate Petri plate surface, and left overnight. During this period, the materials diffused and prevented bacterial growth, creating the appearance of a halo or zone. The maximum size of 15, 12 and 10 mm of zone inhibition emerged around the $\text{Ni}_3\text{S}_4/\text{Ag}_2\text{S}/\text{TiO}_2/\text{CA}$, TiO_2/CA , and $\text{Ag}_2\text{S}/\text{CA}$ materials, respectively, while no zone inhibition occurred around the $\text{Ni}_3\text{S}_4/\text{CA}$ (Figure 14a). The higher antimicrobial activity of the $\text{Ni}_3\text{S}_4/\text{Ag}_2\text{S}/\text{TiO}_2/\text{CA}$ can be explained based on the multiple metals and sulfide in one aerogel which releases more reactive oxygen species (ROS) and kills a higher number of microbial cells [33].

3.3.2. MIC/MBC Analysis

The lowest level or concentration of $\text{Ni}_3\text{S}_4/\text{Ag}_2\text{S}/\text{TiO}_2/\text{CA}$ aerogel materials significantly inhibiting the microbial growth, known as MIC, was found to be approximately between 64 to $128 \mu\text{g}/\text{mL}$ after overnight incubation at 35°C . The bacterial growth was halted by more than 50% at $128 \mu\text{g}/\text{mL}$ concentration of $\text{Ni}_3\text{S}_4/\text{Ag}_2\text{S}/\text{TiO}_2/\text{CA}$ in the growing culture, but sharp growth inhibition was observed from the $64 \mu\text{g}/\text{mL}$ of $\text{Ni}_3\text{S}_4/\text{Ag}_2\text{S}/\text{TiO}_2/\text{CA}$ (Figure 14b). Hence, the MIC value has occurred between these concentrations and is approx. $96 \mu\text{g}/\text{mL}$ of $\text{Ni}_3\text{S}_4/\text{Ag}_2\text{S}/\text{TiO}_2/\text{CA}$ aerogel. The microbial decontamination property of the $\text{Ni}_3\text{S}_4/\text{Ag}_2\text{S}/\text{TiO}_2/\text{CA}$ aerogel increases with the increase of the aerogel dose due to the rise in the active sites in the system. The availability of more active sites releases extra active radicals or species which deactivate the microbe's cell [34].

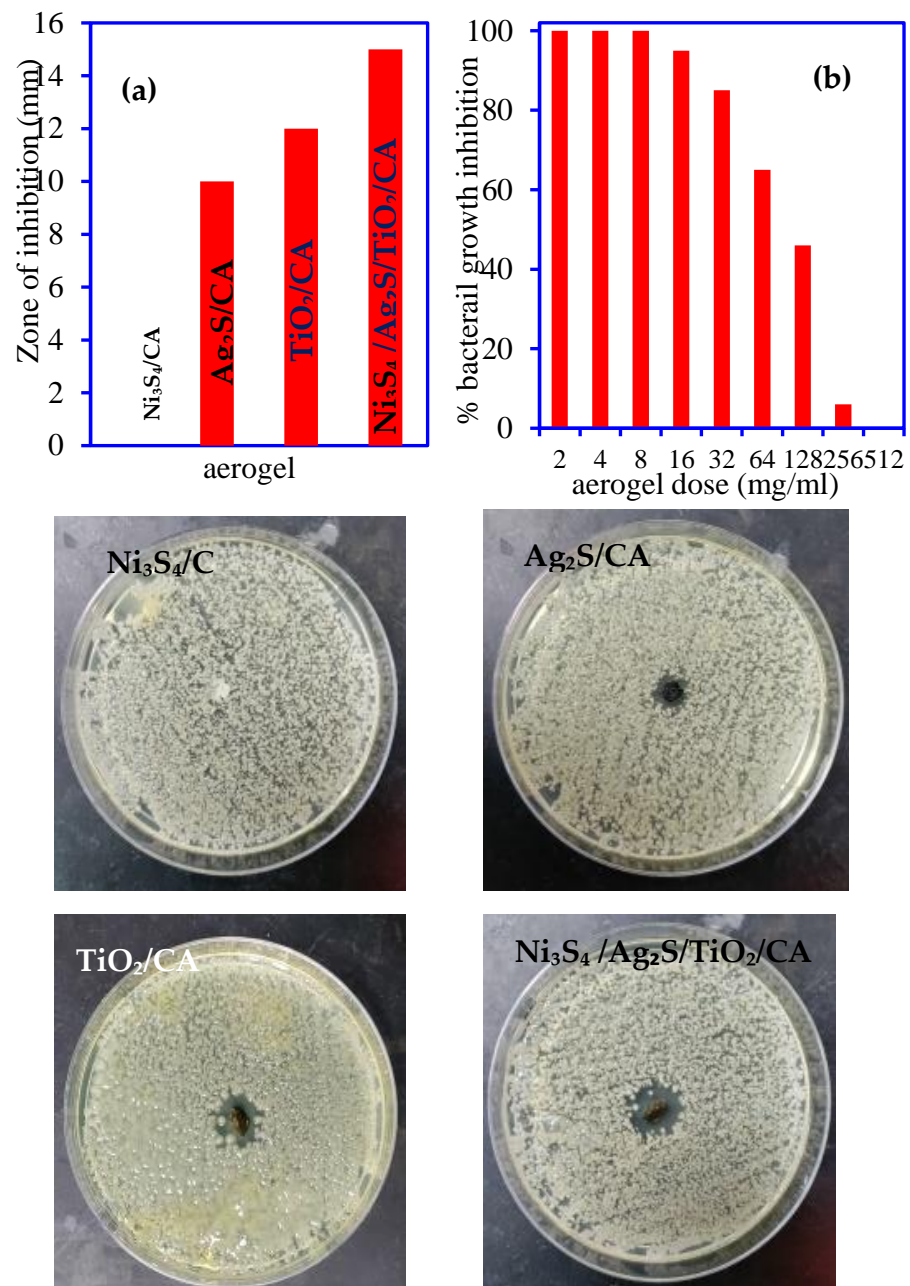


Figure 14. (a) Zone inhibition pattern at 100 µg aerogel concentration (zone inhibition in Petri plate) (b) effect of Ni₃S₄/Ag₂S/TiO₂/CA doses on percent bacterial growth inhibition.

3.3.3. Antimicrobial Mechanism

The antimicrobial results revealed that all the synthesized aerogels except Ni₃S₄/CA prevent the microbes' growth and kill them. The effectiveness of the Ni₃S₄/Ag₂S/TiO₂/CA aerogel was much higher than Ni₃S₄/CA, Ag₂S/CA, and TiO₂/CA aerogels. The mechanism involved in the microbial deactivation activity of the prepared aerogels may include the destruction of the cell integrity after interaction with the aerogel surface and the release of the reactive oxygen species (ROS). Most current studies assume that the interaction of the microbes with the antimicrobial material may inhibit cell wall/membrane synthesis and interrupt energy transduction [35]. Moreover, antimicrobial material may generate ROS through catalysis, which causes enzyme inhibition and DNA damage. Herein, Ni₃S₄/Ag₂S/TiO₂/CA aerogel showed microbial decontamination in darkness and solar light irradiation. Under dark conditions, microbes are trapped on the surface of the aerogel,

and the interaction between metallic moieties and lipid layers of microbes interrupts the cell respiration and cellular pathways [36]. Moreover, surface interaction between aerogel and microbes inhibits biofilm formation, which prevents microbes' further growth [35].

Under solar light illumination, aerogels work more efficiently due to the production of more active charged and radical species like e^- , h^+ , $^-\text{O}_2$, OH , and H_2O_2 . A synergistic effect between Ni_3S_4 , Ag_2S , and TiO_2 in $\text{Ni}_3\text{S}_4/\text{Ag}_2\text{S}/\text{TiO}_2/\text{CA}$ aerogel has been observed and produced more active radical species, increasing the cytotoxicity within the microbe's cell and destroying the nucleic acids [37]. The electron transfer mechanism is also expected to occur for the semiconductor $\text{Ni}_3\text{S}_4/\text{Ag}_2\text{S}/\text{TiO}_2$ in $\text{Ni}_3\text{S}_4/\text{Ag}_2\text{S}/\text{TiO}_2/\text{CA}$ aerogel. The PL analysis (Figure 6) reveals that the PL intensity of the $\text{Ni}_3\text{S}_4/\text{Ag}_2\text{S}/\text{TiO}_2/\text{CA}$ aerogel is low compared to the other synthesized aerogels, reflecting the better separation of charge carriers, e^- , and h^+ [38]. These e^- are absorbed by the cell wall and water molecules and generate ROS. This ROS kills the microbial cells [37,39]. A detailed mechanism of microbial decontamination is shown in Figure 15.

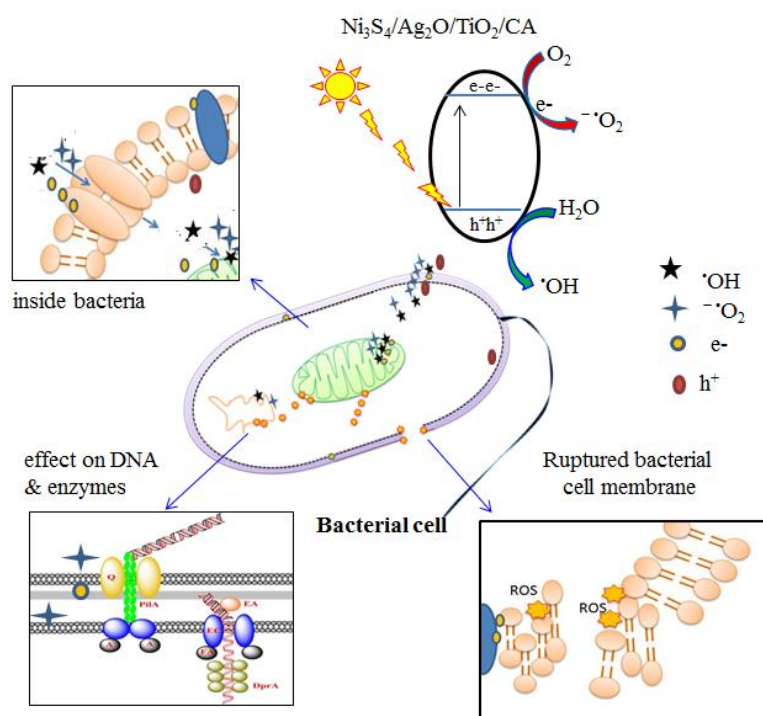


Figure 15. A proposed mechanism for the decontamination of the microbes using $\text{Ni}_3\text{S}_4/\text{Ag}_2\text{S}/\text{TiO}_2/\text{CA}$ aerogel in dark and solar light.

4. Conclusions

This article reports the successful synthesis of the semiconducting $\text{Ni}_3\text{S}_4/\text{CA}$, $\text{Ag}_2\text{S}/\text{CA}$, TiO_2/CA , and $\text{Ni}_3\text{S}_4/\text{Ag}_2\text{S}/\text{TiO}_2/\text{CA}$ aerogels for the adsorptive removal of the OTC drug and microbial decontamination of industrial beverage wastewater in the dark and under solar light illumination. The higher adsorption and antimicrobial properties of the $\text{Ni}_3\text{S}_4/\text{Ag}_2\text{S}/\text{TiO}_2/\text{CA}$ aerogel were mainly due to its surface's multifunctional groups, which have more active sites for interacting with the pollutants. The maximum adsorption of the OTC was observed at pH 6 and within 180 min of equilibrium time. The maximum monolayer adsorption capacity of the $\text{Ni}_3\text{S}_4/\text{Ag}_2\text{S}/\text{TiO}_2/\text{CA}$ aerogel was 29.57 mg/g. The adsorption isotherm and kinetic modeling demonstrated that adsorption of the OCT was chemisorption onto the heterogenous surface of the $\text{Ni}_3\text{S}_4/\text{Ag}_2\text{S}/\text{TiO}_2/\text{CA}$ aerogel. The antimicrobial results of $\text{Ni}_3\text{S}_4/\text{CA}$, $\text{Ag}_2\text{S}/\text{CA}$, TiO_2/CA , and $\text{Ni}_3\text{S}_4/\text{Ag}_2\text{S}/\text{TiO}_2/\text{CA}$ aerogels indicated that all the materials are active in the dark as well as in solar light except the $\text{Ni}_3\text{S}_4/\text{CA}$ aerogel. The zone of inhibition was 10, 12, and 15 mm for $\text{Ni}_3\text{S}_4/\text{Ag}_2\text{S}/\text{TiO}_2/\text{CA}$, $\text{Ag}_2\text{S}/\text{CA}$, and TiO_2/CA , respectively. A synergistic effect between Ni_3S_4 , Ag_2S , and TiO_2 in

Ni₃S₄/Ag₂S/TiO₂/CA aerogel has been observed and produced more active radical species, increasing the cytotoxicity within the microbe's cell and destroying the nucleic acids under the solar light illumination. The photogenerated active charged and radical species such as e⁻, h⁺, -O₂, OH, and H₂O₂ were responsible for the cells' microbial growth inhibition and killing. The present study demonstrated that Ni₃S₄/Ag₂S/TiO₂/CA aerogel is the most efficient of these materials for decontaminating the drug and microbes from the wastewater.

Supplementary Materials: The following supporting information can be downloaded at: <https://www.mdpi.com/article/10.3390/nano12203642/s1>, Figure S1: SEM image of modified TiO₂ (a), Ni₃S₄ (b) and Ag₂S (c). TEM image of modified TiO₂ (d).

Author Contributions: Conceptualization, R.K. and M.A.B.; methodology, R.K. and M.A.B.; validation, M.A.A. and N.H.A.M.; formal analysis, M.O.A.; investigation, M.A.T. and M.O.; resources, M.A.B.; writing—original draft preparation, R.K., M.O.A. and M.O.; writing—review and editing, All authors. All authors have read and agreed to the published version of the manuscript.

Funding: This research work was funded by Institutional Fund Projects under grant no. (IFPRC-182-155-2020). Therefore, authors gratefully acknowledge technical and financial support from the Ministry of Education and King Abdulaziz University, Jeddah, Saudi Arabia.

Data Availability Statement: Not applicable.

Conflicts of Interest: The authors declare no conflict of interest.

References

1. Raffi, M.; Mehrwan, S.; Bhatti, T.M.; Akhter, J.I.; Hameed, A.; Yawar, W. Investigations into the antibacterial behavior of copper nanoparticles against *Escherichia coli*. *Ann. Microbiol.* **2010**, *60*, 75–80. [[CrossRef](#)]
2. Jana, T.; Iqbal, J.; Ismail, M.; Mansoor, Q.; Mahmood, A.; Ahmad, A. Eradication of multi-drug resistant bacteria by Ni doped ZnO nanorods: Structural, raman and optical characteristics. *Appl. Surf. Sci.* **2014**, *308*, 75–81. [[CrossRef](#)]
3. Liu, S.; Kang, L.; Zhang, J.; Jun, S.C.; Yamauchi, Y. Carbonaceous anode materials for nonaqueous sodium- and potassium-ion hybrid capacitors. *ACS Energy Lett.* **2021**, *6*, 4127–4154. [[CrossRef](#)]
4. Chattacharjee, S. Iron sulfide nanoparticles prepared using date seed extract: Green synthesis, characterization and potential application for removal of ciprofloxacin and chromium. *Powder Technol.* **2021**, *380*, 219–228. [[CrossRef](#)]
5. Kromah, V.; Zhang, G. Aqueous adsorption of heavy metals on metal sulfide nanomaterials: Synthesis and application. *Water* **2021**, *13*, 1843. [[CrossRef](#)]
6. Liu, Y.; Wang, H.; Yuan, X.; Wu, Y.; Wang, H.; Tan, Y.Z.; Chew, J.W. Roles of sulfur-edge sites, metal-edge sites, terrace sites, and defects in metal sulfides for photocatalysis. *Chem. Catal.* **2021**, *1*, 44–68. [[CrossRef](#)]
7. Kumar, N.; Mittal, H.; Parashar, V.; Sinha Ray, S.; Ngila, J.C. Efficient removal of rhodamine 6G dye from aqueous solution using nickel sulphide incorporated polyacrylamide grafted gum karaya bionanocomposite hydrogel. *RSC Adv.* **2016**, *6*, 21929–21939. [[CrossRef](#)]
8. Hosseini, M.; Fazelian, N.; Fakhri, A.; Kamyab, H.; Yadav, K.K.; Chelliapan, S. Preparation, and structural of new NiS-SiO₂ and Cr₂S₃-TiO₂ nano-catalyst: Photocatalytic and antimicrobial studies. *J. Photochem. Photobiol. B Biol.* **2019**, *194*, 128–134. [[CrossRef](#)]
9. Pang, M.; Hu, J.; Zeng, H.C. Synthesis, Morphological Control, and Antibacterial Properties of Hollow/Solid Ag₂S/Ag Heterodimers. *J. Am. Chem. Soc.* **2010**, *132*, 10771–10785. [[CrossRef](#)]
10. Zhang, H.; Chen, M.; Wang, D.; Xu, L.; Liu, X. Laser induced fabrication of mono-dispersed Ag₂S@Ag nano-particles and their superior adsorption performance for dye removal. *Opt. Mater. Express* **2016**, *6*, 2573–2583. [[CrossRef](#)]
11. Gupta, V.K.; Fakhri, A.; Agarwal, S.; Azad, M. Synthesis and characterization of Ag₂S decorated chitosan nanocomposites and chitosan nanofibers for removal of Lincosamides antibiotic. *Int. J. Biol. Macromol.* **2017**, *103*, 1–7. [[CrossRef](#)]
12. Wang, B.; Wan, Y.; Zheng, Y.; Lee, X.; Liu, T.; Yu, Z.; Huang, J.; Ok, Y.S.; Chen, J.; Gao, B. Alginate-based composites for environmental applications: A critical review. *Crit. Rev. Environ. Sci. Technol.* **2019**, *49*, 318–356. [[CrossRef](#)]
13. Li, J.; Liu, J.; Sun, Q.; Banis, M.N.; Sun, X.; Sham, T.-K. Tracking the effect of sodium insertion/extraction in amorphous and anatase TiO₂ nanotubes. *J. Phys. Chem. C* **2017**, *121*, 11773–11782. [[CrossRef](#)]
14. Kumar, R. Mixed phase lamellar titania-titanate anchored with Ag₂O and polypyrrole for enhanced adsorption and photocatalytic activity. *J. Colloid Interf. Sci.* **2016**, *477*, 83–93. [[CrossRef](#)]
15. Ansari, M.O.; Khan, M.M.; Ansari, S.A.; Lee, J.; Cho, M.H. Enhanced thermoelectric behaviour and visible light activity of Ag@TiO₂/polyaniline nanocomposite synthesized by biogenic-chemical route. *RSC Adv.* **2014**, *4*, 23713–23719. [[CrossRef](#)]
16. Nawaz, M.; Khan, A.A.; Hussain, A.; Jang, J.; Jung, H.Y.; Lee, D.S. Reduced graphene oxide -TiO₂/sodium alginate 3-dimensional structure aerogel for enhanced photocatalytic degradation of ibuprofen and sulfamethoxazole. *Chemosphere* **2020**, *261*, 127702. [[CrossRef](#)]

17. Fan, C.; Chen, C.; Wang, J.; Fu, X.; Ren, Z.; Qian, G.; Wang, Z. Black Hydroxylated Titanium Dioxide Prepared via Ultrasonication with Enhanced Photocatalytic Activity. *Sci. Rep.* **2015**, *5*, 11712. [[CrossRef](#)]
18. Peng, L.; Doménech-Carbó, A.; Primo, A.; García, H. 3D defective graphenes with subnanometric porosity obtained by soft-templating following zeolite procedures. *Nanoscale Adv.* **2019**, *1*, 4827–4833. [[CrossRef](#)]
19. Kao, C.W.; Wu, P.T.; Liao, M.Y.; Chung, I.J.; Yang, K.C.; Tseng, W.Y.; Yu, J. Magnetic nanoparticles conjugated with peptides derived from monocyte chemoattractant protein-1 as a tool for targeting atherosclerosis. *Pharmaceutics* **2018**, *10*, 62. [[CrossRef](#)]
20. Zhu, L.; Lu, Q.; Lv, L.; Wang, Y.; Hu, Y.; Deng, Z.; Lou, Z.; Hou, Y.; Teng, F. Ligand-free rutile and anatase TiO₂ nanocrystals as electron extraction layers for high performance inverted polymer solar cells. *RSC Adv.* **2017**, *7*, 20084–20092. [[CrossRef](#)]
21. Karthikeyan, R.; Thangaraju, D.; Prakash, N.; Hayakawa, Y. Single-step synthesis and catalytic activity of structure-controlled nickel sulfide nanoparticles. *Cryst. Eng. Comm.* **2015**, *17*, 5431–5439. [[CrossRef](#)]
22. Park, G.D.; Cho, J.S.; Kang, Y.C. Sodium-ion storage properties of nickel sulfide hollow nanospheres/reduced graphene oxide composite powders prepared by a spray drying process and the nanoscale Kirkendall effect. *Nanoscale* **2015**, *7*, 16781–16788. [[CrossRef](#)] [[PubMed](#)]
23. Dai, T.; Wan, Y.; Tian, R.; Wang, S.; Han, T.; Wang, G. In situ cation exchange generated ZnS–Ag₂S nanoparticles for photothermal detection of transcription factor. *ACS Appl. Bio Mater.* **2020**, *3*, 3260–3267. [[CrossRef](#)] [[PubMed](#)]
24. Lach, J.; Ociepa-Kubicka, A.; Mrowiec, M. Oxytetracycline Adsorption from Aqueous Solutions on Commercial and High-Temperature Modified Activated Carbons. *Energies* **2021**, *14*, 3481. [[CrossRef](#)]
25. Wang, Y.; Zhou, J.; Bi, W.; Qin, J.; Wang, G.; Wang, Z.; Fu, P.; Liu, F. Schwertmannite catalyze persulfate to remove oxytetracycline from wastewater under solar light or UV-254. *J. Clean. Prod.* **2022**, *364*, 132572. [[CrossRef](#)]
26. Zhang, X.; Lin, X.; He, Y.; Chen, Y.; Luo, X.; Shang, R. Study on adsorption of tetracycline by Cu-immobilized alginate adsorbent from water environment. *Int. J. Biol. Macromol.* **2019**, *124*, 418–428. [[CrossRef](#)]
27. Liu, W.; Shen, X.; Han, Y.; Liu, Z.; Dai, W.; Dutta, A.; Kumar, A.; Liu, J. Selective adsorption and removal of drug contaminants by using an extremely stable Cu(II)-based 3D metal-organic framework. *Chemosphere* **2019**, *215*, 524–531. [[CrossRef](#)]
28. Luo, H.; Liu, Y.; Lu, H.; Fang, Q.; Rong, H. Efficient Adsorption of Tetracycline from Aqueous Solutions by Modified Alginate Beads after the Removal of Cu(II) Ions. *ACS Omega* **2021**, *6*, 6240–6251. [[CrossRef](#)]
29. Eniola, J.O.; Kumar, R.; Al-Rashdi, A.A.; Barakat, M.A. Hydrothermal synthesis of structurally variable binary CuAl, MnAl and ternary CuMnAl hydroxides for oxytetracycline antibiotic adsorption. *J. Environ. Chem. Eng.* **2020**, *8*, 103535. [[CrossRef](#)]
30. Fideles, R.A.; Ferreira, G.M.D.; Teodoro, F.S.; Adarme, O.F.H.; da Silva, L.H.M.; Gil, L.F.; Gurgel, L.V.A. Trimellitated sugarcane bagasse: A versatile adsorbent for removal of cationic dyes from aqueous solution. Part I: Batch adsorption in a monocomponent system. *J. Colloid Interface Sci.* **2018**, *515*, 172–188. [[CrossRef](#)]
31. Kajjumba, G.W.; Emik, S.; Öngen, A.; Özcan, H.K.; Aydın, S. Modelling of Adsorption Kinetic Processes—Errors, Theory and Application. In *Advanced Sorption Process Applications*; Edebali, S., Ed.; Intech Open: London, UK, 2018.
32. Yang, Z.; Chen, C.; Li, B.; Zheng, Y.; Liu, X.; Shen, J.; Zhang, Y.; Wu, S. A core-shell 2DMoS₂@MOF hetero-structure for rapid therapy of bacteria-infected wounds by enhanced photocatalysis. *Chem. Eng. J.* **2022**, *451*, 139127. [[CrossRef](#)]
33. Kiani, M.; Bagherzadeh, M.; Kaveh, R.; Rabiee, N.; Fatahi, Y.; Dinarvand, R.; Jang, H.W.; Shokouhimehr, M.; Varma, R.S. Novel Pt-Ag₃PO₄/CdS/chitosan nanocomposite with enhanced photocatalytic and biological activities. *Nanomaterials* **2020**, *10*, 2320. [[CrossRef](#)]
34. Packirisamy, R.G.; Govindasamy, C.; Sanmugam, A.; Karuppasamy, K.; Kim, H.S.; Vikraman, D. Synthesis and antibacterial properties of novel ZnMn₂O₄-chitosan nanocomposites. *Nanomaterials* **2019**, *9*, 1589. [[CrossRef](#)]
35. Shaikh, S.; Nazam, N.; Rizvi, S.M.D.; Ahmad, K.; Baig, M.H.; Lee, E.J.; Choi, I. Mechanistic insights into the antimicrobial actions of metallic nanoparticles and their implications for multidrug resistance. *Int. J. Mol. Sci.* **2019**, *20*, 2468. [[CrossRef](#)]
36. Geraldo, D.A.; Arancibia-Miranda, N.; Villagra, N.A.; Mora, G.C.; Arratia-Perez, R. Synthesis of CdTe QDs/single-walled aluminosilicate nanotubes hybrid compound and their antimicrobial activity on bacteria. *J. Nanoparticle Res.* **2012**, *14*, 1–9. [[CrossRef](#)]
37. Shahri, N.N.M.; Taha, H.S.A.; Hamid, M.H.; Kusriani, E.; Lim, J.W.; Hobley, J.; Usman, A. Antimicrobial activity of silver sulfide quantum dots functionalized with highly conjugated Schiff bases in a one-step synthesis. *RSC Adv.* **2022**, *12*, 3136–3146. [[CrossRef](#)]
38. Rui, J.; Deng, N.; Zhao, Y.; Tao, C.; Zhou, J.; Zhao, Z.; Huang, X. Activation of persulfate via Mn doped Mg/Al layered double hydroxide for effective degradation of organics: Insights from chemical and structural variability of catalyst. *Chemosphere* **2022**, *302*, 134849. [[CrossRef](#)]
39. Patra, P.; Roy, S.; Sarkar, S.; Mitra, S.; Pradhan, S.; Debnath, N.; Goswami, A. Damage of lipopolysaccharides in outer cell membrane and production of ROS-mediated stress within bacteria makes nano zinc oxide a bactericidal agent. *Appl. Nanosci.* **2015**, *5*, 857–866. [[CrossRef](#)]